# Observation of the Leggett-Rice Effect in a Unitary Fermi Gas

S. Trotzky,[1] S. Beattie,[1] C. Luciuk,[1] S. Smale,[1] A. B. Bardon,[1] T. Enss,[2] E. Taylor,[3] S. Zhang,[4] and J. H. Thywissen[1,5]
[1]Department of Physics, University of Toronto, Ontario M5S 1A7, Canada
[2]Institut für Theoretische Physik, Universität Heidelberg, 69120 Heidelberg, Germany
[3]Department of Physics and Astronomy, McMaster University, Hamilton, Ontario L8S 4M1, Canada
[4]Department of Physics, Center of Theoretical and Computational Physics, University of Hong Kong, Hong Kong, China
[5]Canadian Institute for Advanced Research, Toronto, Ontario M5G 1Z8, Canada
(Received 5 November 2014; published 7 January 2015)

We observe that the diffusive spin current in a strongly interacting degenerate Fermi gas of $^{40}$K precesses about the local magnetization. As predicted by Leggett and Rice, precession is observed both in the Ramsey phase of a spin-echo sequence, and in the nonlinearity of the magnetization decay. At unitarity, we measure a Leggett-Rice parameter $\gamma = 1.08(9)$ and a bare transverse spin diffusivity $D_0^\perp = 2.3(4)\hbar/m$ for a normal-state gas initialized with full polarization and at one-fifth of the Fermi temperature, where $m$ is the atomic mass. One might expect $\gamma = 0$ at unitarity, where two-body scattering is purely dissipative. We observe $\gamma \to 0$ as temperature is increased towards the Fermi temperature, consistent with calculations that show the degenerate Fermi sea restores a nonzero $\gamma$. Tuning the scattering length $a$, we find that a sign change in $\gamma$ occurs in the range $0 < (k_F a)^{-1} \lesssim 1.3$, where $k_F$ is the Fermi momentum. We discuss how $\gamma$ reveals the effective interaction strength of the gas, such that the sign change in $\gamma$ indicates a switching of branch between a repulsive and an attractive Fermi gas.

DOI: 10.1103/PhysRevLett.114.015301 PACS numbers: 67.85.Lm, 67.10.Jn, 75.76.+j

Transport properties of unitary Fermi gases have been studied extensively in the past few years. Because of strong interparticle interactions at unitarity, various transport coefficients like viscosity and spin diffusivity are bounded [1–3] by a conjectured quantum minimum [4–6], in three dimensions. On the other hand, transport in two-dimensional unitary Fermi gases shows anomalous behavior, apparently violating a quantum limit [7]. This remains to be understood.

In the case of spin diffusion, experiments so far [2,3,7] have been interpreted with a spin current proportional to the magnetization gradient, $\boldsymbol{J}_j = -D\nabla_j \boldsymbol{M}$, where $D$ is the diffusion constant [8], and $\boldsymbol{M} = \langle M_x, M_y, M_z \rangle$ is the local magnetization. Bold letters indicate vectors in Bloch space and the subscript $j \in \{1, 2, 3\}$ denotes spatial direction. In general, $\boldsymbol{J}_j$ has both a longitudinal component $\boldsymbol{J}_j^\parallel \parallel \boldsymbol{M}$ and a transverse component $\boldsymbol{J}_j^\perp \perp \boldsymbol{M}$. Longitudinal spin currents are purely dissipative, and the standard diffusion equation applies [5,6,9,10]. However, as Leggett and Rice pointed out [11], the transverse spin current follows

$$\boldsymbol{J}_j^\perp = -D_{\mathrm{eff}}^\perp \nabla_j \boldsymbol{M} - \gamma \boldsymbol{M} \times D_{\mathrm{eff}}^\perp \nabla_j \boldsymbol{M}, \qquad (1)$$

where $D_{\mathrm{eff}}^\perp = D_0^\perp/(1 + \gamma^2 M^2)$ is the effective transverse diffusivity and $\gamma$ is the Leggett-Rice (LR) parameter [12] [see Fig. 1(a)]. Physically, the second term describes a reactive component of the spin current that precesses around the local magnetization. This precession has been observed in weakly interacting Fermi gases [7,13,14] and is a manifestation of the so-called identical spin-rotation effect [15], which is intimately related to the LR effect [16]. In a unitary Fermi gas, however, neither the existence of the LR effect nor the value of $\gamma$ has been measured. In this Letter, we provide the first evidence for LR effects in a unitary Fermi gas, and measure $\gamma$ using a spin-echo technique.

Our experiments are carried out in a trapped cloud of $^{40}$K atoms using the two lowest-energy Zeeman states $|\pm z\rangle$ of the electronic ground-state manifold [17]. Interactions between these states are tuned by the Feshbach resonance [21] at 202.1 G. We start with a completely spin-polarized sample in the lowest-energy state $|-z\rangle$. This large initial

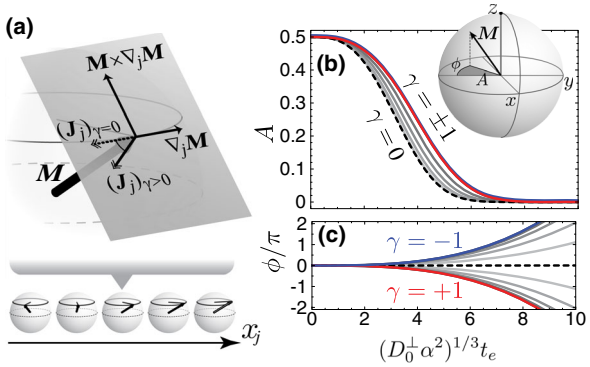


FIG. 1 (color online). The Leggett-Rice effect. (a) In a transverse spin spiral along $x_j$, the gradient $\nabla_j \boldsymbol{M} \perp \boldsymbol{M}$ drives a spin current $\boldsymbol{J}_j \perp \boldsymbol{M}$, as described by Eq. (1). For $\gamma \neq 0$, $\boldsymbol{J}_j$ is rotated around $\boldsymbol{M}$ by $\arctan(\gamma)$ compared to $(J_j)_{\gamma=0}$. In a spin-echo experiment, this causes both a slower decay of amplitude, $A = |M_x + iM_y|$ shown in (b), as well as an accumulated phase, $\phi = -\arg(iM_x - M_y)$ shown in (c). The case of $\theta = 5\pi/6$ and full initial polarization is plotted. Dashed lines in (b) and (c) show $\gamma = 0$, and gray lines show steps of 0.2 up to $\gamma = \pm 1$.

 

polarization enhances the LR effect, since $\gamma$ appears as a product with $M$ in the equations of motion. Polarization also suppresses the critical temperature of superfluidity [22,23] to below the temperature range explored here.

We probe magnetization dynamics using a series of radio-frequency (rf) pulses. At time $t = 0$, a resonant pulse with area $\theta$ creates a superposition of $|-z\rangle$ and $|+z\rangle$, in which $M_z = -\cos(\theta)$ and $M_{xy} \equiv M_x + iM_y = i\sin(\theta)$. During time evolution, a controlled magnetic-field gradient $B' = 17.0(7)$ G/cm oriented along the $x_3$ spatial direction leads to a variation of the phase of the superposition, twisting the $xy$ magnetization $M_{xy}$ into a spiral. After a spin-refocusing pulse ($\pi_x$) at time $t_\pi$, the spiral untwists, and all spins realign at the echo time $t_e = 2t_\pi$. A readout $\pi/2$ pulse with variable phase lag closes an internal-state interferometer, which is observed using time-of-flight imaging after Stern-Gerlach state separation [17]. The contrast and phase of interference fringes measure the trap-averaged values of both the amplitude $A = |M_{xy}|$ and phase $\phi = -\arg(iM_{xy})$ of the $xy$ magnetization at the echo time.

In such an echo experiment, $M_z$ is manipulated only by rf pulses, and is otherwise conserved globally and even locally in a uniform system. However the gradient of $M_{xy}$ initializes irreversible spin currents that cause the transverse magnetization to decay. The resulting dynamics are described by [11]

$$\partial_t M_{xy} = -i\alpha x_3 M_{xy} + D_{\rm eff}^{\perp}(1 + i\gamma M_z)\nabla_3^2 M_{xy}, \quad (2)$$

where $\alpha = B'\Delta\mu/\hbar$, and $\Delta\mu$ is the difference in magnetic moment between $|+z\rangle$ and $|-z\rangle$.

If $\gamma = 0$, the solution of Eq. (2) is $A(t_e) = A_0 \exp(-D_0^{\perp}\alpha^2 t_e^3/12)$ [8]. For $\gamma \neq 0$, but for small $A_0$ or short times, $A(t_e)$ decays with the same functional form but with $D_0^{\perp}$ replaced by $D_{\rm eff}^{\perp} < D_0^{\perp}$. At longer times, however, the magnetization loss can differ significantly from this simple form. The full solution to Eq. (2) is given by

$$A(t_e) = A_0\sqrt{\frac{1}{\eta}\mathcal{W}\left(\eta\exp\left[\eta - \frac{D_0^{\perp}\alpha^2 t_e^3}{6(1+\gamma^2 M_z^2)}\right]\right)}, \quad (3)$$

$$\phi(t_e) = \gamma M_z \ln\left(\frac{A(t_e)}{A_0}\right), \quad (4)$$

where $\eta = \gamma^2 A_0^2/(1+\gamma^2 M_z^2)$ and $\mathcal{W}(z)$ is the Lambert-$W$ function. Figures 1(b) and 1(c) show typical plots of Eqs. (3) and (4) for a variety of $\gamma$. The LR effect is seen in both amplitude and phase dynamics. However, $A(t_e)$ alone is an ambiguous signature. For example, a similar shape of $A(t_e)$ could result from a magnetization dependence of $D_0^{\perp}$, as is predicted to occur below the so-called anisotropy temperature due to restrictions of collisional phase space [9,24]. The evolution of $\phi(t_e)$ and its relation to $A(t_e)$, on the other hand, are unique features of the LR effect that are sensitive to the signs of $\gamma$ and $M_z$.

Figure 2(a) shows the measured $A(t_e)$ and $\phi(t_e)$ at unitarity and initial temperature $(T/T_F)_i \simeq 0.2$, for three initial-pulse areas, where $T_F$ is the Fermi temperature. We test for the LR effect by plotting $\phi(t_e)$ as a function of $M_z \ln(A/A_0)$ [see Fig. 2(b)], where $A_0$ is obtained by extrapolating $A(t_e)$ to $t_e = 0$ and full initial polarization is assumed, i.e., $M_z^2 + A_0^2 = 1$. We determine $\gamma$ from a linear fit to the data plotted as in Fig. 2(b), following Eq. (4). Fixing $\gamma$, diffusivity is determined from a subsequent fit of Eq. (3) to $A(t_e)$ [lines in Fig. 2(a)]. From this analysis, we obtain $\gamma = 1.08(9)$ and $D_0^{\perp} = 2.3(4)\hbar/m$ at unitarity. These best-fit transport coefficients should be regarded as an average over the trapped ensemble, and over the full range of magnetization. Furthermore, during the spin diffusion process, temperature rises due to demagnetization [3,25]. Full demagnetization at unitarity increases $T/T_F$ from 0.2 to about 0.4, but the temperature rises less for smaller pulse angles and for weaker interactions.

At low temperature, Landau Fermi liquid (LFL) theory [26] provides a microscopic interpretation of these transport parameters: $D_0^{\perp} = 2\chi_0\tau_{\perp}\epsilon_F/(3m^*\chi)$, where $\tau_{\perp}$ is the transport lifetime, $\epsilon_F = (\hbar k_F)^2/2m$ is the local Fermi energy of an ideal gas, $\chi$ is the magnetic susceptibility, and $\chi_0$ is its ideal-gas value, and $m^*$ is the effective mass. The LR parameter is $\gamma = -(4\chi_0/3\chi)(\tau_{\perp}\epsilon_F/\hbar)\lambda$, with $\lambda \equiv -\hbar\gamma/(2m^* D_0^{\perp})$ a dimensionless coefficient. The thermodynamic response of the system is parametrized by LFL parameters $F_{0,1}^{a,s}$: $m^* = m(1+F_1^s/3)$, $\chi m/m^* = \chi_0/(1+F_0^a)$, and $\lambda = (1+F_0^a)^{-1} - (1+F_1^a/3)^{-1}$ [11,26]. However, $\tau_{\perp}$ is accessible only by transport measurements. If we use the $D_0^{\perp}$ at our lowest probed temperature, with $\chi/\chi_0 = 0.73$ and $m^*/m = 1.13$ from a thermodynamic measurement [27], we estimate $\tau_{\perp} \approx 2.5\hbar/\epsilon_F$. Since LFL theory assumes $\tau_{\perp} \gg \hbar/\epsilon_F$, the transport lifetime we find is at or near the lower self-consistent bound for a quasiparticle treatment [28].

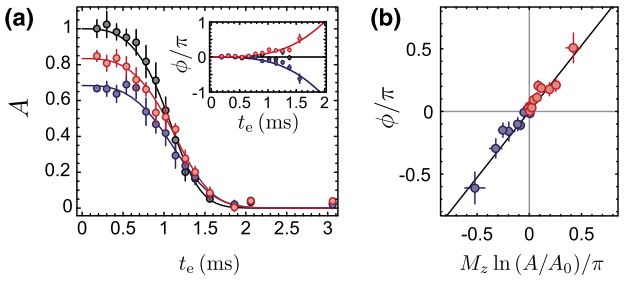


FIG. 2 (color online). (a) Amplitude $A$ and phase $\phi$ (inset) of the $xy$ magnetization measured at unitarity for $(T/T_F)_i \simeq 0.2$ and with $M_z = 0.00(5)$ (black circles), $M_z = 0.74(2)$ (blue), and $M_z = -0.54(3)$ (red). All data are taken at a spin-echo time. Error bars represent uncertainties from the fit to a full interferometric fringe. (b) Plot of $\phi(t_e)$ versus $M_z \ln[A(t_e)/A_0]$ for the two cases where $M_z \neq 0$. The solid line is a linear fit to both data sets that is used to extract $\gamma$. Error bars represent combined uncertainties from fit and extrapolation. The solid lines in (a) represent fits with Eq. (3) using the value of $\gamma$ obtained by the analysis presented in (b).

Notice that $\lambda$ has two contributions: $F_0^a$, corresponding to the effective magnetic field produced by local magnetization, and $F_1^a$, corresponding to a spin vector potential created by a local spin current. The latter has no analogue for weakly interacting fermions. A spin-echo experiment such as ours can constrain $F_1^a$, if all other LFL parameters are known. We find $\lambda \approx -0.2$ at unitarity, smaller in magnitude than $2.1 \leq \lambda \leq 2.7$ in liquid $^3$He [29]. Combined with $F_0^a = 1.1(1)$ from thermodynamic measurements, this implies $F_1^a \approx 0.5$ for a unitary Fermi gas. Repeating our measurements at smaller magnetization and lower temperature would provide a test of LFL theory for a unitary gas. For instance, our estimated value of $F_1^a$ is near the upper limit to be consistent with $F_1^s = 0.4(1)$ determined from $m^*$ in a balanced gas [27], since LFL theory requires $F_1^a < F_1^s$ [30].

Figures 3 and 4 show how spin transport depends on temperature and interaction strength. We reinterpret our earlier work [3] to have observed the effective diffusivity $D_{\mathrm{eff}}^{\perp}$; whereas here we find both $\gamma$ and the bare $D_0^{\perp}$. Within the range of parameters explored, $D_0^{\perp}$ is still consistent with the conjectured limit [4–6].

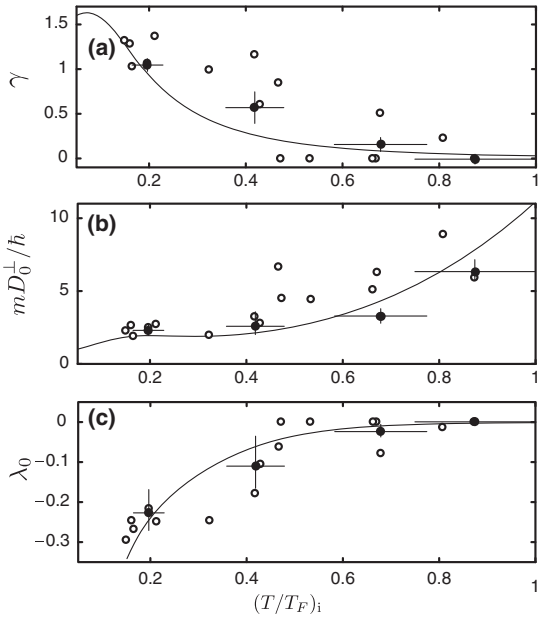


FIG. 3. Spin transport at unitarity. (a) The measured LR parameter $\gamma$, (b) diffusivity $D_0^{\perp}$, and (c) the ratio $\lambda_0 = -\hbar\gamma/(2mD_0^{\perp})$ are shown versus the initial reduced temperature $(T/T_F)_i$. Solid points are each from a phase-sensitive measurement as shown in Fig. 2. Horizontal and vertical error bars represent statistical and fit uncertainties. For these data, $N$ ranges from $50(5) \times 10^3$ at low temperature to $18(4) \times 10^3$ at high temperature. Open circles are results from a fit of Eq. (3) to $\theta \simeq \pi/2$ data such as the black circles in Fig. 2(a), and also to data from Ref. [3]. Here, we fix $M_z$ and vary $\gamma$ (chosen *a posteriori* to be non-negative) and $D_0^{\perp}$. Although the two methods provide similar values on average, the phase-sensitive measurements provide reduced scatter for $\gamma \lesssim 0.5$, and are sensitive to the sign of $\gamma$. Solid lines show a kinetic theory calculation in the limit of large imbalance, and using the local reduced temperature at peak density [17].

We compare our data to a kinetic theory [17,24] in which collisions are described in terms of the many-body $T$ matrix $\mathcal{T}(\vec{q}, \omega)$, which gives the low-energy effective interaction between fermions near the Fermi surface, whose center-of-mass momentum and energy are $\hbar\vec{q}$ and $\hbar\omega$, respectively [17]. Kinetic theory relates $\gamma$ to a momentum average of $\mathcal{T}$ [17,24]; this result is shown in Figs. 3 and 4. At low temperatures, $\mathcal{T}$ is peaked about $\vec{q} = 0$, $\omega = 0$, and $\gamma$ is well approximated by $\gamma = -\mathrm{Re}\mathcal{T}(\vec{0}, 0)\tau_{\perp} n/\hbar$, where $n$ is number density [9]. We use this to interpret some of our results in what follows. A simple interpretation of $\mathcal{T}$ is given by its weakly interacting limit in vacuum, $\mathcal{T} \to -(4\pi\hbar^2/m)f(k)$, where $f(k) = -1/(a^{-1} + ik)$ is the $s$-wave scattering amplitude, $a$ is the $s$-wave scattering length, and $k$ is the relative wave vector of two colliding fermions. More generally, the sign of $\mathrm{Re}\mathcal{T}$ reveals whether dressed interactions in the gas are attractive or repulsive [17].

The conceptual simplicity of $\lambda$ is that the ratio $-\gamma/D_0^{\perp}$ eliminates $\tau_{\perp}$, leaving a quantity proportional to $\mathrm{Re}\mathcal{T}$. However, $m^*$ is not known for the full range of

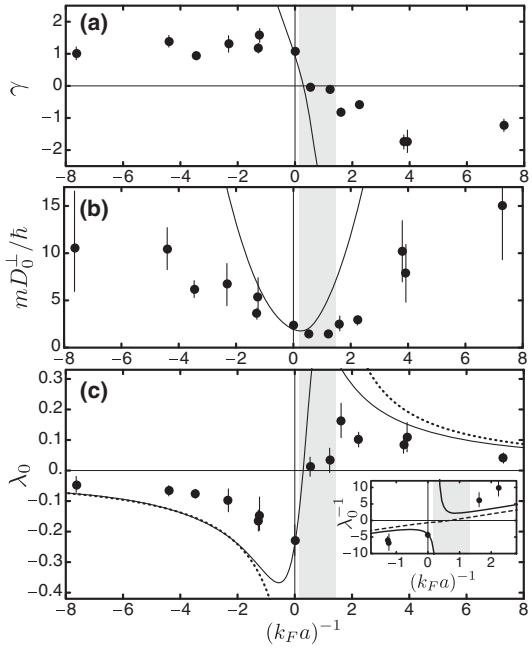


FIG. 4. Effect of interaction strength on spin transport. (a) LR parameter $\gamma$, (b) $D_0^{\perp}$, and (c) $\lambda_0$ as a function of $(k_F a)^{-1}$. The error bars represent fit uncertainties. For these data, $(T/T_F)_i = 0.18(4)$ and $N = 40(10) \times 10^3$, where uncertainty is due to number variation between runs. In the range $0 < (k_F a)^{-1} \lesssim 1.3$ (indicated in gray) both free atoms and Feshbach dimers are present, as discussed in the text and in Fig. 5. Solid lines show a kinetic theory calculation [17] at $(T/T_F)_i = 0.20$; the dotted line in (c) shows the weakly interacting limit $\lambda_0 = [\pi/(2k_F a) - 1]^{-1}$ for a balanced $T = 0$ gas [16]. The inset to (c) shows $\lambda_0^{-1}$, and includes a calculation using the momentum averaged upper branch $T$ matrix (solid line) as well as $\lambda_0^{-1} = (4\epsilon_F/3n)\mathcal{T}^{-1}(\vec{0}, 0)$. The sign change of $\lambda_0$ at $0.4 \leq (k_F a)^{-1} \leq 1$ is a robust feature of theory, and is consistent with our data.

polarizations, temperatures, and interaction strengths probed here. We report instead $\lambda_0 \equiv -\hbar\gamma/(2mD_0^\perp) \propto \mathrm{Re}\mathcal{T}(\vec{0},0)$ with the bare mass [31]. The pair $D_0^\perp$ and $\lambda_0$ encapsulate the dissipative and reactive effects of scattering.

At unitarity, we observe that $\lambda_0$ depends sensitively on $(T/T_F)_i$ and approaches zero at high temperatures [Fig. 3(c)]. This is in contrast to the temperature insensitivity of spin-wave behavior in a weakly interacting Fermi gas [13]. At high temperatures, $\mathcal{T}$ reduces to the two-body scattering amplitude mentioned above, which is purely imaginary at unitarity. As a result, $\lambda_0$ approaches zero. At low temperature, however, the degenerate Fermi sea restores a nonzero $\mathrm{Re}\mathcal{T}$ and, hence, $\lambda_0$.

For all interaction strengths in Fig. 4, data are analyzed as described above for unitarity. However, the validity of our hydrodynamic model likely breaks down at weaker interactions. We estimate that the mean free path $\ell \approx 3D_0/k_F$ at peak density changes from 300 nm at $(k_Fa)^{-1} \approx 0$ to 3 $\mu$m at $|k_Fa|^{-1} = 2$. This approaches both the pitch of the spin spiral, $1/\alpha t \approx 4$ $\mu$m at $t_e \sim 1$ ms, and the Thomas-Fermi radius of the cloud, 5 $\mu$m, along the $x_3$ direction. Thus, we expect the data analysis based on Eq. (1) to be most accurate in the strongly interacting regime.

Figure 4(a) shows an approximately linear change in $\gamma$ across $-1 \le (k_Fa)^{-1} \le 3$. This agrees only qualitatively with our kinetic calculation (solid line). However, the calculation is for full and constant polarization, and does not encompass the dynamic temperature, nor the inhomogeneous density of the cloud. A second salient feature of the data is the minimum in $D_0^\perp$ near the scattering resonance, which is reminiscent of behavior seen in other transport parameters [2,7,32]. Strong collisions impede the transport of spin. As with $\gamma$, the best-fit $D_0^\perp$ saturates at larger $|k_Fa|^{-1}$, perhaps due to finite-size effects that remain to be understood.

The LR effect changes sign in the range $0 < (k_Fa)^{-1} \lesssim 1.3$ [see Figs. 4(a) and 4(c)]. This indicates that the effective interaction between fermions changes sign as one tunes the system across the Feshbach resonance [17]. Such a sign change is only possible if the system switches from the "upper branch" of the energy spectrum near the Feshbach resonance [33–36] to the lower branch, in which interactions are attractive.

The sign change of $\mathrm{Re}\mathcal{T}(\vec{0},0)$ has been previously discussed [37,38] in the context of an upper-branch instability, in which atoms decay to form bound pairs in the lower branch [39–41]. To search for dimers that would be produced by the pairing instability, we use a combination of magnetoassociation and spin-flip spectroscopy (Fig. 5). We observe that for $0 < (k_Fa)^{-1} \lesssim 1.3$, the same range of $(k_Fa)^{-1}$ where $\gamma$ changes sign, there are weakly bound Feshbach dimers, even though $a > 0$ for the entire experimental sequence. We shade this range in Fig. 4, to flag the simultaneous presence of upper- and lower-branch atoms. No clear evidence of Feshbach dimers appears at $(k_Fa)^{-1} \ge 1.3$; however, more deeply bound dimers would not appear in our detection method [40].

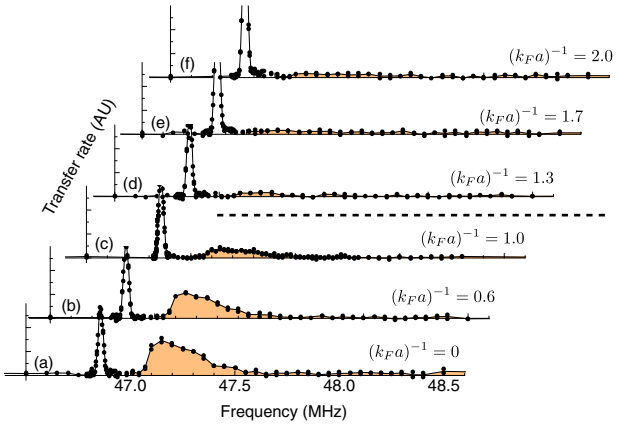


FIG. 5 (color online). Presence of dimers above the Feshbach resonance. At the indicated initial $(k_Fa)^{-1}$, a superposition is created with $\theta = \pi/2$ and held for 3 ms. The field is then swept to 200.0 G in 5 ms, which magnetoassociates some lower-branch pairs into dimers with a binding energy of $h \times 200$ kHz. Dimers are identified with their rf dissociation spectrum, using an 80-$\mu$s pulse near the 46.85 MHz spin-flip resonance from the $|+z\rangle$ state to a previously unoccupied Zeeman state [42]. Each plot shows the transfer rate versus rf frequency. For traces (a), (b), and (c), there is a clearly identified molecular feature above 47.0 MHz (spectral weight shaded in orange). However for traces (d), (e), and (f), the spectral weight above 47.0 MHz is insensitive to field, and consistent with the noise of the measurement.

In summary, we have observed an unambiguous signature of the Leggett-Rice effect in a strongly interacting Fermi gas. In the limit of zero temperature, $\gamma$ and $D_0^\perp$ are scale-invariant universal transport parameters of the unitary Fermi gas. The value of $D_0^\perp$ reveals the strength of dissipative scattering in the gas. It is near the proposed quantum limit, such that the inferred value of $\tau_\perp$ is comparable to the "Planck time" $\hbar/\epsilon_F$ [43]. This raises the possibility that incoherent transport may play a role, i.e., that a quasiparticle-based picture may be incomplete.

The Leggett-Rice effect reveals the reactive component of scattering between fermions of unlike spin. The nonzero value of $\gamma$ tells us that spin waves in a unitary Fermi gas are dispersive [44], or in other words, that the gas has a spin stiffness in the long-wavelength limit [45,46]. Spin stiffness is an essential ingredient of ground-state magnetic textures [47]. Even though magnetic ordering does not occur in the conditions of our experiments, this same energetic term is clearly observed with our interferometric measurement.

We thank E. Demler, R. Ragan, and A. Paramekanti for stimulating conversations, and N. Zuber for experimental assistance. This work was supported by NSERC, by AFOSR under FA9550-13-1-0063, by ARO under W911NF-14-1-0282, and by RGC under HKU-709313P.

[1] C. Cao, E. Elliott, J. Joseph, H. Wu, J. Petricka, T. Schäfer, and J. E. Thomas, Science **331**, 58 (2011).

[2] A. Sommer, M. Ku, G. Roati, and M. W. Zwierlein, Nature (London) **472**, 201 (2011); A. Sommer, M. Ku, and M. W. Zwierlein, New J. Phys. **13**, 055009 (2011).

[3] A. B. Bardon, S. Beattie, C. Luciuk, W. Cairncross, D. Fine, N. S. Cheng, G. J. A. Edge, E. Taylor, S. Zhang, S. Trotzky, and J. H. Thywissen, Science **344**, 722 (2014).

[4] P. K. Kovtun, D. T. Son, and A. O. Starinets, Phys. Rev. Lett. **94**, 111601 (2005); T. Schäfer and D. Teaney, Rep. Prog. Phys. **72**, 126001 (2009); T. Enss, R. Haussmann, and W. Zwerger, Ann. Phys. (Amsterdam) **326**, 770 (2011).

[5] G. M. Bruun, New J. Phys. **13**, 035005 (2011).

[6] T. Enss and R. Haussmann, Phys. Rev. Lett. **109**, 195303 (2012).

[7] M. Koschorreck, D. Pertot, E. Vogt, and M. Köhl, Nat. Phys. **9**, 405 (2013).

[8] E. L. Hahn, Phys. Rev. **80**, 580 (1950); H. Y. Carr and E. M. Purcell, Phys. Rev. **94**, 630 (1954); H. C. Torrey, Phys. Rev. **104**, 563 (1956).

[9] J. W. Jeon and W. J. Mullin, Phys. Rev. Lett. **62**, 2691 (1989); W. J. Mullin and J. W. Jeon, J. Low Temp. Phys. **88**, 433 (1992); A. Meyerovich, Phys. Lett. A **107**, 177 (1985); A. E. Meyerovich and K. A. Musaelian, Phys. Rev. Lett. **72**, 1710 (1994).

[10] D. Wulin, H. Guo, C.-C. Chien, and K. Levin, Phys. Rev. A **83**, 061601 (2011); G. M. Bruun and C. J. Pethick, Phys. Rev. Lett. **107**, 255302 (2011); H. Heiselberg, Phys. Rev. Lett. **108**, 245303 (2012); M. P. Mink, V. P. J. Jacobs, H. T. C. Stoof, R. A. Duine, M. Polini, and G. Vignale, Phys. Rev. A **86**, 063631 (2012); H. Kim and D. A. Huse, Phys. Rev. A **86**, 053607 (2012); O. Goulko, F. Chevy, and C. Lobo, New J. Phys. **14**, 073036 (2012); T. Enss, C. Küppersbusch, and L. Fritz, Phys. Rev. A **86**, 013617 (2012); O. Goulko, F. Chevy, and C. Lobo, Phys. Rev. Lett. **111**, 190402 (2013).

[11] A. J. Leggett and M. J. Rice, Phys. Rev. Lett. **20**, 586 (1968); A. J. Leggett, J. Phys. C **3**, 448 (1970).

[12] The relation of $\gamma$ to the conventional LR parameter $\mu$ is $\gamma = n\mu/2$.

[13] X. Du, L. Luo, B. Clancy, and J. E. Thomas, Phys. Rev. Lett. **101**, 150401 (2008); X. Du, Y. Zhang, J. Petricka, and J. E. Thomas, Phys. Rev. Lett. **103**, 010401 (2009).

[14] J. Heinze, J. S. Krauser, N. Flaschner, K. Sengstock, C. Becker, U. Ebling, A. Eckardt, and M. Lewenstein, Phys. Rev. Lett. **110**, 250402 (2013).

[15] F. Piéchon, J. N. Fuchs, and F. Laloë, Phys. Rev. Lett. **102**, 215301 (2009); S. S. Natu and E. J. Mueller, Phys. Rev. A **79**, 051601 (2009).

[16] K. Miyake, W. J. Mullin, and P. C. E. Stamp, J. Phys. (Paris) **46**, 663 (1985).

[17] See Supplemental Material at http://link.aps.org/supplemental/10.1103/PhysRevLett.114.015301, which includes Refs. [18–20], for further details of experimental and theoretical methods.

[18] H. Akimoto, D. Candela, J. S. Xia, W. J. Mullin, E. D. Adams, and N. S. Sullivan, Phys. Rev. Lett. **90**, 105301 (2003).

[19] T. Enss, Phys. Rev. A **86**, 013616 (2012).

[20] C. A. R. Sá de Melo, M. Randeria, and J. R. Engelbrecht, Phys. Rev. Lett. **71**, 3202 (1993).

[21] C. Chin, R. Grimm, P. Julienne, and E. Tiesinga, Rev. Mod. Phys. **82**, 1225 (2010).

[22] B. S. Chandrasekhar, Appl. Phys. Lett. **1**, 7 (1962); A. M. Clogston, Phys. Rev. Lett. **9**, 266 (1962).

[23] Y.-I. Shin, C. H. Schunck, A. Schirotzek, and W. Ketterle, Nature (London) **451**, 689 (2008).

[24] T. Enss, Phys. Rev. A **88**, 033630 (2013).

[25] R. Ragan, K. Grunwald, and C. Glenz, J. Low Temp. Phys. **126**, 163 (2002).

[26] G. Baym and C. J. Pethick, *Landau Fermi-Liquid Theory: Concepts and Applications* (Wiley-VCH, New York, 1991).

[27] S. Nascimbène, N. Navon, K. J. Jiang, F. Chevy, and C. Salomon, Nature (London) **463**, 1057 (2010); S. Nascimbène, N. Navon, S. Pilati, F. Chevy, S. Giorgini, A. Georges, and C. Salomon, Phys. Rev. Lett. **106**, 215303 (2011).

[28] X. Deng, J. Mravlje, R. Žitko, M. Ferrero, G. Kotliar, and A. Georges, Phys. Rev. Lett. **110**, 086401 (2013).

[29] D. S. Greywall, Phys. Rev. B **27**, 2747 (1983).

[30] A. J. Leggett, Ann. Phys. (N.Y.) **46**, 76 (1968).

[31] For theory curves, we use $\chi m^*/m\chi_0 = 1$, which is correct in the weakly interacting limit but introduces a systematic error for an interacting gas, on the order of 20% for the balanced, low-temperature unitary gas.

[32] E. Elliott, J. A. Joseph, and J. E. Thomas, Phys. Rev. Lett. **113**, 020406 (2014); M. Bluhm and T. Schäfer, Phys. Rev. A **90**, 063615 (2014).

[33] L. Pricoupenko and Y. Castin, Phys. Rev. A **69**, 051601 (2004).

[34] S. Pilati, G. Bertaina, S. Giorgini, and M. Troyer, Phys. Rev. Lett. **105**, 030405 (2010).

[35] S.-Y. Chang, M. Randeria, and N. Trivedi, Proc. Natl. Acad. Sci. U.S.A. **108**, 51 (2011).

[36] V. B. Shenoy and T.-L. Ho, Phys. Rev. Lett. **107**, 210401 (2011).

[37] D. Pekker, M. Babadi, R. Sensarma, N. Zinner, L. Pollet, M. W. Zwierlein, and E. Demler, Phys. Rev. Lett. **106**, 050402 (2011).

[38] I. Sodemann, D. A. Pesin, and A. H. MacDonald, Phys. Rev. A **85**, 033628 (2012).

[39] C. Sanner, E. J. Su, W. Huang, A. Keshet, J. Gillen, and W. Ketterle, Phys. Rev. Lett. **108**, 240404 (2012); Y.-R. Lee, M.-S. Heo, J.-H. Choi, T. T. Wang, C. A. Christensen, T. M. Rvachov, and W. Ketterle, Phys. Rev. A **85**, 063615 (2012).

[40] S. Zhang and T.-L. Ho, New J. Phys. **13**, 055003 (2011).

[41] X. Cui and H. Zhai, Phys. Rev. A **81**, 041602 (2010); G. J. Conduit and E. Altman, Phys. Rev. A **82**, 043603 (2010); P. N. Ma, S. Pilati, M. Troyer, and X. Dai, Nat. Phys. **8**, 601 (2012); S. Pilati, I. Zintchenko, and M. Troyer, Phys. Rev. Lett. **112**, 015301 (2014).

[42] C. A. Regal, C. Ticknor, J. L. Bohn, and D. S. Jin, Nature (London) **424**, 47 (2003).

[43] S. A. Hartnoll, arXiv:1405.3651; J. A. N. Bruin, H. Sakai, R. S. Perry, and A. P. Mackenzie, Science **339**, 804 (2013).

[44] V. P. Silin, Zh. Eksp. Teor. Fiz. **33**, 1227 (1957) [Sov. Phys. JETP **6**, 945 (1958)].

[45] V. P. Mineev, Phys. Rev. B **72**, 144418 (2005).

[46] E. Demler (private communication).

[47] I. Berdnikov, P. Coleman, and S. H. Simon, Phys. Rev. B **79**, 224403 (2009); L. J. LeBlanc, J. H. Thywissen, A. A. Burkov, and A. Paramekanti, Phys. Rev. A **80**, 013607 (2009).